ACS SENSORS

pubs.acs.org/acssensors

Article

Small RNA Biosensor Design Strategy To Mitigate Off-Analyte Response

Nicholas E. Larkey, Jessica L. Phillips, Hyo Sang Jang, Siva K. Kolluri, and Sean M. Burrows*

Cite This: *ACS Sens.* 2020, 5, 377−384

Read Online

ACCESS | Metrics & More | Article Recommendations | Supporting Information

ABSTRACT: Several bottlenecks in the design of current sensor technologies for small noncoding RNA must be addressed. The small size of the sensors and the large number of other nucleotides that may have sequence similarity makes selectivity a real concern. Many of the current sensors have one strand with an exposed region called a toehold. The toehold serves as a place for the analyte nucleic acid strand to bind and initiate competitive displacement of sensors' secondary strands. Since the toehold region is not protected, any endogenous oligonucleotide sequences that are similar or only different by a few nucleic acids will interact with the toehold and cause false signals. To address sensor selectivity, we investigated how the toehold location in the sensor impacts the sensitivity and selectivity for the analyte of interest. We will discuss the differences in sensitivity and selectivity for a miR-146a-5p biosensor in the presence of different naturally occurring mismatch sequences. We found that altering the toehold location lowered the rate of the false signal from off-analyte microRNA by upward of 20 percentage points. Detection limits as low as 56 pM were observed when the sensor concentration was 5 nM. The findings herein are broadly applicable to other small and large RNAs as well as other types of sensing platforms.

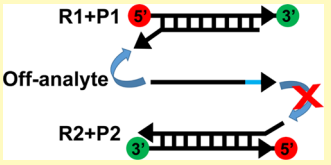

KEYWORDS: *nucleic acids, microRNA, nanostructure, toehold mediated strand displacement, fluorescence*

Biosensors are designed to selectively interact with specific biomolecules and relay information about the corresponding biological processes. One type of a regulatory biomolecule that has been gaining popularity is microRNA (miR). miRs are short (18−25 nucleotides) noncoding RNA.[1] Some miRs are involved with the progression of various types of cancer.[2−13] Our goal was to innovate the design of fluorescent biosensors to detect miR and other small noncoding RNAs.

Conventional nucleic acid biosensors rely on sequence complementarity between the sensor and the analyte.[14] An overarching problem in the nucleic acid biosensor field is the limits of thermodynamics on differentiating between strands with similar sequences to the analyte-of-interest. Graybill and Bailey state in their 2016 review of miR biosensors that high sequence selectivity is of utmost importance because the differences in the sequence between analyte miR and off-analyte miRs can be as little as a single nucleotide.[15] Some researchers have developed techniques to differentiate single-nucleotide polymorphism binding based on differences in fluorescence emission.[16−18] Since the binding mechanism was not selective for any particular analyte, in the limit of low analyte concentration and high off-analyte concentration, selectivity for the analyte will become problematic. Zhang et al. have designed nucleic acid strands called protector + complement probes that can specifically differentiate between nucleic acid strands but relies on linear sequences that displace a quenching mechanism. Unfortunately, quencher-based signaling methods are known to be susceptible to nuclease degradation.[19,20]

We have previously developed a double-stranded "reporter + probe" biosensor that has a reporter strand partially bound to a probe strand.[21] In the presence of the analyte, the probe strand will preferentially bind the analyte, displacing the reporter molecule through toehold-mediated strand-displacement. The freed reporter then forms a stem-loop conformation. This change in conformation of the reporter molecule moves two dyes closer to each other, creating a measurable change in fluorescence intensity that is proportional to the analyte concentration. The benefit of bringing the dyes together is to lower false signals from sensor degradation, unlike fluorescence recovery via disrupting a quenching mechanism.[21,22] The rationale is that the chances for false signals from unintentionally separating the dyes is much higher than unintentionally bringing them together.

In previous iterations of the reporter + probe biosensor, we have shown how thermodynamics is important when designing displacement-based miR biosensors, and how different dyes and different spacer lengths between the dye and distal ends of the reporter strand alter and improve the signal generated by the sensors.[21−25] Previous works on toehold thermodynamics have laid the foundation for this field,[19] and novel techniques to regulate strand displacement with blocking strands have

Received: October 7, 2019
Accepted: January 16, 2020
Published: January 16, 2020

been made. The reporter + probe biosensor design that we established has recently been gaining popularity with other researchers adapting the design for the detection of human telomerase RNA.[26]

The previous reporter + probe biosensors that we have designed[21,24,25] were able to resist off-analytes that were different from the analyte sequences (at least three nucleotide mismatches). The design requires that the thermodynamic stability for the binding between the probe and off-analytes be unfavorable. However, we have yet to study how the directionality of the biosensor's toehold can be tuned in order to decrease binding by off-analytes with similar sequences. Previous kinetic simulations for RNA strand-displacement have shown that toeholds located on the 5′ end of the substrate rather than the 3′ can be faster because of additional cross-stacking interaction.[27] However, when considering sensor selectivity, the location of the toehold is important to the nature of how the analyte and off-analytes initiate binding to the sensor. Here, we studied this issue by designing biosensors that had the unprotected toehold region in different locations. The hypothesis was that if mismatched base pairs between the probe's toehold and the off-analyte weaken the binding interaction between them, then, the stability of the displacement initiation region will decrease.[19] Thus, the weaker binding will discourage the displacement of the reporter from the probe. To test the hypothesis, we designed two biosensors with different molecular configurations. In one biosensor, the toehold contained only bases that were complementary to the analyte and not the off-analyte. The other biosensor's configuration had the probe's toehold complementary to both the analyte and off-analyte. The fluorescence signal was monitored in the presence of analyte and off-analyte.

In this study, the reporter + probe biosensors were designed for miR-146a-5p, a miR shown to be either upregulated or downregulated with respect to various cancers and has the potential to become a biomarker for these diseases.[28−31] Outside of cancer, miR-146a has recently been found to be an important fibroblast regulator in the development of arthritis.[32] Here, we tested different reporter + probe biosensors for their selectivity toward miR-146a-5p and their sensitivity in a complex sample matrix (raw cell lysate). The off-analytes that we tested against here were miR-146a-3p and miR-146b-5p, two miRs with similar sequences to the analyte. The results from these studies are not limited to miR-146a-5p and are broadly applicable to other small and large RNA.

EXPERIMENTAL SECTION

Thermodynamic Predictions and Calculations. Equilibrium, thermodynamic, and structural metrics were assessed to determine the biosensors' ability to properly function and achieve selectively for the analyte. UNAfold, a web server utilizing a "dynamic programming algorithm", was used for all thermodynamic calculations.[33,34] Further details on the parameters and boundary values for these functions can be found in the Supporting Information Section S-1 ("Thermodynamic Parameters").

Off-Analyte Discovery. Off-analytes were found with miRBase, a miR database operated by the University of Manchester.[35−37] Details on the process for finding off-analytes and the results of this search can be found in Supporting Information Section S-2 ("Off-Analyte Discovery Process") and Figures S1−S3.

Biosensor Design. Reporter + probe biosensors were designed to be sensitive and selective toward miR hsa-miR-146a. In order to increase the reporter fluorescence resonance energy transfer (FRET) enhancement, internal poly-ethylene glycol (PEG) spacers (hexaethylene glycol) were placed between the nucleic acids and the dyes on both the 5′ and 3′ ends.[25] The analyte and off-analyte miR sequences were converted to DNA analogues for testing because DNA resists nuclease degradation better than RNA.

DNA was purchased from Integrated DNA Technologies (Coralville, IA) and used as received. Concentrations of DNA in the working solutions were determined with a Nanodrop spectrophotometer (ND-1000). Details on the DNA sequences, samples, stock solutions, working solutions, and logic behind the biosensor design is in Supporting Information Section S-3 ("Biosensor Design Details") and Table S1.

For the remainder of this work, reporter 1 and reporter 2 are referred to as R1 and R2, respectively. Similarly, probe 1 and probe 2 will be referred to as P1 and P2, respectively. The analyte and off-analyte sequences will be shortened as well with miR-146a-5p, miR-146a-3p, and miR-146b-5p becoming analyte (A), off-analyte1 (OA1), and off-analyte2 (OA2), respectively.

Fluorimeter Design. A custom-built fluorimeter excited the samples and collected the fluorescence spectra, and was described previously.[21] Samples were excited with 250 mW of 935 nm laser light. This wavelength and power were experimentally determined to give the highest FRET enhancement (from eq S1) for the fluorescein| ATTO 633 dye pair in R1 (Supporting Information, Figure S4) and were consistent with previous biosensors having similar dyes.[25] Details on the fluorimeter, Lightfield software, and data collection are located in Supporting Information Section S-4, "Spectroscopic Information".

Cell Lysate. MCF-7 cells were kindly donated by Dr. Emily Ho at Oregon State University. MCF-7 cell lysate was prepared with a freeze-thaw method adapted from Doyle et al. and previously used by our group.[38,39] Details on the cell culture and the freeze-thaw method are located in Supporting Information Section S-5 ("Cell Lysate Details"). The cell lysate was thawed prior to experiments and diluted in the previously described buffer ("Biosensor Design") down to 1×10^6 lysed cells per mL.

Off-Analyte Testing. To form the respective reporter + probe complexes, reporters (R1 and R2) were prehybridized with equimolar amounts of their respective probes (P1 and P2) in a microcentrifuge tube at 37 °C for 4 h. Next, aliquots of one of these newly formed reporter + probe complexes or a reporter control were added to microcentrifuge tubes containing enough analyte or off-analyte to be either 1× (5 nM) or 10× (50 nM). Each tube was then diluted with buffer (described in "Biosensor Design" section) to a final reporter + probe concentration of 5 nM (with either 5 or 50 nM analyte/off-analyte). These samples were placed back at 37 °C for at least 1 h before fluorescence data were collected. From these solutions, the measured intensities from R + P and R-hairpin were used to determine FRET quenching (eq 1) and FRET enhancement (eq 2) values for each of the reporter + probe biosensors.

The following equation calculated the percent change in the signal for quenching (% ΔS_Q)

$$\% \Delta S_Q = 100 \times \frac{S_{R+P} - S_R}{S_{R+P}} \quad (1)$$

The following equation calculated the percent change in the signal for enhancement (% ΔS_E)

$$\% \Delta S_E = 100 \times \frac{S_R - S_{R+P}}{S_{R+P}} \quad (2)$$

The S value was the summed signal over a prescribed emission range. More information for emission ranges for summation can be found in the Supporting Information Section S-2 ("Spectroscopic Information").

Calibration Curves. Reporter + probe complexes were prehybridized as described in "Off-Analyte Testing". Aliquots of reporter + probe were added to microcentrifuge tubes containing increasing amounts of analyte. Each tube was then diluted with buffer containing MCF-7 cell lysate (see "Cell Lysate" section above) to a final reporter

https://dx.doi.org/10.1021/acssensors.9b01968
ACS Sens. 2020, 5, 377−384

+ probe concentration of 5 nM, and the analyte concentration ranged from 0 to 15 nM. These samples were placed back at 37 °C for at least 1 h before collecting fluorescence data. A linear calibration curve was fit to the linear region from 0 to 5 nM analyte. A control solution of 5 nM reporter was made to compare to the 5−15 nM analyte solutions. Each reporter type and each calibration curve (with control solutions) were conducted at least three separate times (N = 3). Excitation and collection parameters are identical with those in "Fluorimeter Design" and "Off-Analyte Testing" sections as well as the Supporting Information Section S-2 ("Spectroscopic Information").

RESULTS AND DISCUSSION

Biosensor's Toehold Location. Two reporter + probe biosensors (R1 + P1 and R2 + P2) were designed to be sensitive and selective for the analyte miR-146a-5p. We evaluated how the sensors' toehold location on the probe would impact off-analyte response and maintain nanomolar or lower sensitivity. The off-analytes were miR-146a-3p and miR-146b-5p. For the remainder of the text, we will refer to miR-146a-5p as "analyte" or "A", miR-146a-3p as "off-analyte1 (OA1)", and miR-146b-5p as "off-analyte2 (OA2)".

For comparative sensor design, care was taken to ensure that R1 and R2 as well as R1 + P1 and R2 + P2 were as similar as possible, both in the number of bound nucleotides for the reporter + probe complex and in thermodynamic stability. Biosensors R1 + P1 and R2 + P2 differ only where the toehold was exposed for the analyte to initiate binding. For R1 + P1, the toehold was such that the 3′ end of the probe (P1) was exposed. In this configuration, the 5′ ends of analytes and off-analytes bind to the toehold. For R2 + P2, the opposite occurs, with the toehold such that the 5′ end of the probe was exposed. In this case, the 3′ ends of analytes and off-analytes bind to the toehold (Scheme 1 and Figure 1).

Scheme 1. Comparing the Binding Initiation of OA2 (miR-146b-5p) to Probes for Both R1 + P1 and R2 + P2 Reporter + Probe Biosensors; Two-Nucleotide Polymorphism in OA2 Was Located Near the 3′ End of the Molecule

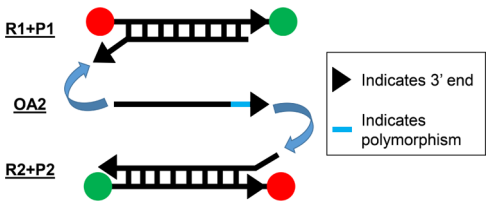

Off-analyte1 (miR-146a-3p, OA1) was dissimilar to the analyte, and little binding between probes and off-analyte1 was predicted. The two reporter + probe designs were primarily created to test differences in selectivity against off-analyte2 (miR-146b-5p, OA2) because of the two polymorphisms in the 3′ end of the strand. As seen in Table S1 (of Supporting Information Section S-3 "Biosensor Design Details") comparing analyte to off-analyte2, the polymorphisms occur in nucleotides 18 (G to A) and 21 (T to C). We hypothesized that having the toehold exposed to off-analyte2's polymorphic region would introduce destabilizing forces to inhibit binding between off-analyte2 and the probe's toehold. In this way, the reporter was less likely to be displaced. If this was the case, then, the signal change in the presence of off-analytes was expected to be minimal.

The thermodynamic stabilities relevant to the reporter + probe biosensors are in Table S2. Differences in the

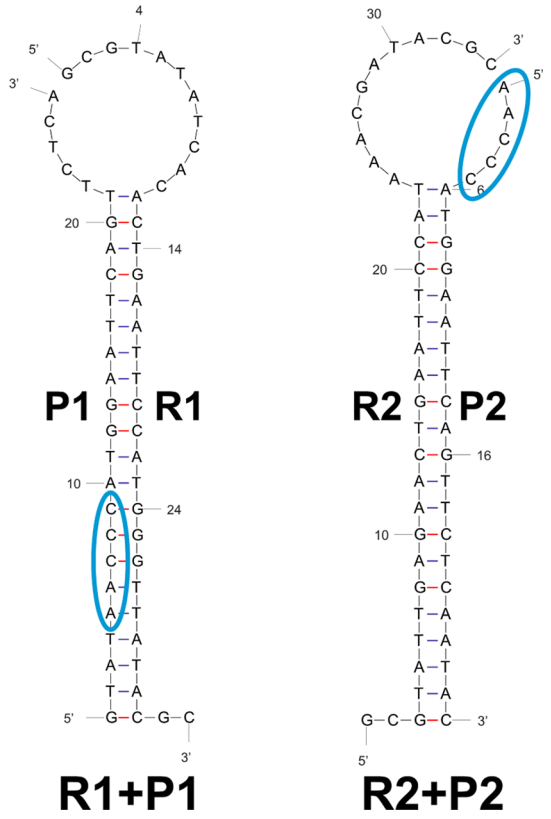

Figure 1. Predicted binding structures for reporter + probe biosensors R1 + P1 and R2 + P2. Blue oval indicates the location of the probe region that will bind to the polymorphic region of off-analyte miR-146b-5p. Structures were calculated from "two state melting (hybridization)" application in UNAfold, with parameters presented in Supporting Information Section S-1 ("Thermodynamic Parameters").

thermodynamic stabilities of the reporter hairpins and reporter + probe complexes for the two designs were kept under 1 kcal/mol (see Supporting Information, Figure S5 for the predicted binding structures of both reporter-hairpins). We designed both probes to have a similar binding response with the analyte or the off-analytes. The difference between the two probes' sequences was the additional four nucleotides added to either the 5′ (in the case of P1) or 3′ (in the case of P2) ends of the probes. The extra nucleotides bind with one of reporter's stems, and this four-nucleotide region was designed to have no interaction with the analyte or off-analytes analyzed.

As seen in Table S2, there was no thermodynamic difference calculated between P1 + off-analyte2 and P2 + off-analyte2 (both have a calculated Gibb's energy of −15.6 kcal/mol). Similarly, there was no difference between P1 + off-analyte1 and P2 + off-analyte1 (both have a calculated Gibb's energy of −3.4 kcal/mol). There was a slight difference in the binding energy between P1 and P2 for the analyte (by ∼0.6 kcal/mol in Gibbs energy). The slight difference was most likely due to the nearest neighbor effect.[40] Although there was a small difference, P1 + analyte and P2 + analyte were still comparable. More extensive thermodynamic calculations can be found in Supporting Information Figures S6 through S10 and Tables S3 through S5.

From equimolar R-hairpin and R + P experiments outlined in the Experimental Section "Off-Analyte Testing", we determined how much the fluorescein signal was quenched

https://dx.doi.org/10.1021/acssensors.9b01968
ACS Sens. 2020, 5, 377−384

when in the hairpin conformation. Similarly, we determined how much the ATTO 633 signal was enhanced by FRET from fluorescein. The fluorescent spectra showing quenching and enhancement for R1/R1 + P1 are found in Figure 2.

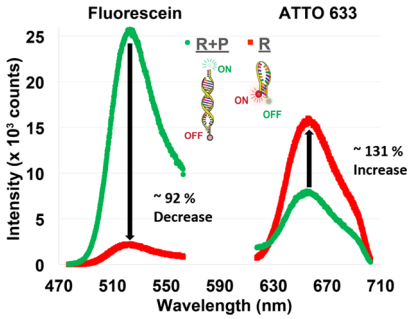

Figure 2. Signal change between equimolar R1 + P1 and R1-hairpin for both donor and acceptor dyes.

R1/R1 + P1 had better quenching ability than R2/R2 + P2, by ∼7 percentage points (Table 1). Conversely, R2/R2 + P2

Table 1. Percent Quenching ΔS_Q and Percent Enhancement ΔS_E (N = 3)

	ΔS_Q ± STDEV	ΔS_E ± STDEV
R1/R1 + P1	92.42 ± 0.13	130.96 ± 3.07
R2/R2 + P2	85.33 ± 0.41	212.14 ± 5.78

had better enhancement ability than R1/R1 + P1 by ∼81 percentage points (Table 1). Equations 1 and 2, calculated quenching and enhancement, respectively. These equations are outlined in the "Off-Analyte Testing" section above.

Biosensor Selectivity. For selectivity experiments, equimolar amounts of analyte or off-analytes were added to the reporter + probe complexes. Additionally, a 10× concentration of off-analyte2 (miR-146b-5p) was added to assess the selectivity with an excess of off-analyte, a common challenge in RNA analysis. In Figure 3, the analyte caused the most signal change for each R + P complex (R1 + P1 and R2 + P2, signal change: decrease in the signal from R + P to R-hairpin for fluorescein and increase in the signal from R + P to R-hairpin for ATTO 633). As discussed in detail below, false signals from off-analytes ranged from 1 to 40%. Together, these results indicated that the sensors were more sensitive to analyte than to the two off-analytes.

For off-analyte1 (miR-146a-3p), the fluorescein signal from R1 + P1 had no statistical difference between R1 + P1 and R1 + P1 + off-analyte1 (p > 0.05, N = 3). Similarly, for ATTO 633, there was no statistical difference (p > 0.05, N = 3) between the signal for R1 + P1 and R1 + P1 + off-analyte1. These results mean off-analyte1 did not cause R1 + P1 to have a false signal.

For off-analyte2, the 1× and 10× additions to R1 + P1 caused a statistical decrease in the fluorescein signal by ∼4.8 and ∼21%, respectively (p < 0.05, N = 3). Looking at the ATTO 633 signal for 1× and 10× additions of off-analyte2 (R1 + P1 + off-analyte2), the signal statistically increased by ∼7.0 and ∼27%, respectively, when compared to R1 + P1 (p < 0.05, N = 3).

For R2 + P2, there was no statistical difference in the signal for R2 + P2 and R2 + P2 + off-anayte1 (p > 0.05, N = 3). Similarly, for ATTO 633, there was no statistical difference in

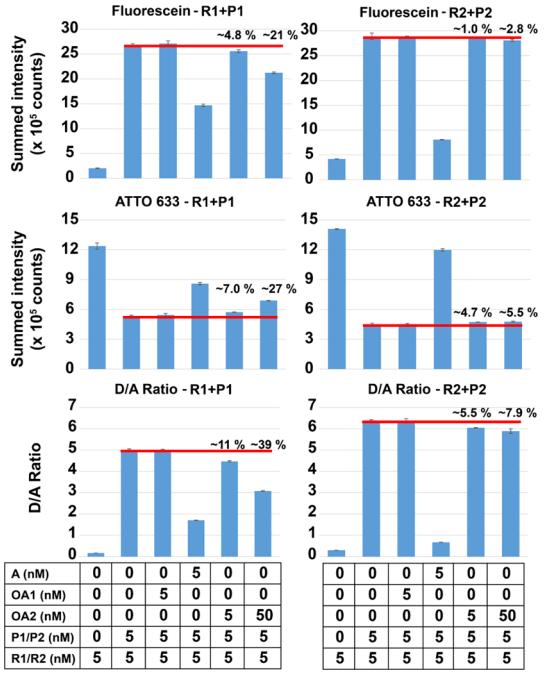

Figure 3. Selectivity tests for R1 + P1 and R2 + P2 with analyte and off-analytes. Either 1× or 10× OA2 was added to determine the concentration effect on the signal change.

the signal for R2 + P2 and R2 + P2 + off-analyte1 (p > 0.05, N = 3). Like R1 + P1, R2 + P2 did not have any false signals from off-analyte1.

For the 1× and 10× additions of off-analyte2 to R2 + P2 (R2 + P2 + off-analyte2), the respective decreases in the fluorescein signal were ∼1.0 and ∼2.8%, but these were not statistically significant from R2 + P2 (p > 0.05, N = 3). For the 1× and 10× additions of off-analyte2 (R2 + P2 + off-analyte2), increases of ∼4.8 and ∼5.5% in the ATTO 633 signal were seen when compared to R2 + P2; both were statistically different (p < 0.05, N = 3).

In response to both the 1× and 10× additions of off-analyte2, fluorescein experienced less signal change on R2 + P2 than on R1 + P1. Moreover, fluorescein's signal from R2 + P2 did not have a statistical response to off-analyte2 at 1× and 10× additions as that was seen for R1 + P1. For ATTO 633, the R2 + P2 signal increase from 1× and 10× off-analyte2 (4.7 and 5.5%, respectively) was less than that of R1 + P1 (7.0 and 27%, respectively). These results demonstrate that R2 + P2 did a better job mitigating binding to off-analyte2 than R1 + P1.

When analyzing the D/A ratio, there was no significant difference between R1 + P1 and R1 + P1 + off-analyte1. For the 1× and 10× additions of off-analyte2, the D/A ratios showed a statistically significant decrease by ∼11 and ∼39%, respectively, compared to R1 + P1 (p < 0.05, N = 3).

For R2 + P2, there was no statistical difference in the D/A ratio for R2 + P2 and R2 + P2 + off-analyte1 (p > 0.05, N = 3). For the 1× and 10× additions of off-analyte2 (R2 + P2 + off-analyte2), the D/A ratio showed a statistically significant decrease of ∼5.5 and ∼7.9%, respectively, compared to R2 + P2 (p < 0.05, N = 3). Although both R1 + P1 and R2 + P2 had D/A ratio responses to off-analyte2, R2 + P2 had less change in the D/A ratio than R1 + P1 (for both the 1× and 10× additions of off-analyte2). These results further demonstrate how changing the location of sensors' toehold region discourages binding with off-analytes.

https://dx.doi.org/10.1021/acssensors.9b01968
ACS Sens. 2020, 5, 377−384

Additional experiments were performed with 10× off-analyte1 for R1 + P1 and R2 + P2 (Supporting Information, Figure S11). Neither the fluorescein signal nor the D/A ratio showed any statistical difference between the R + P + 10× off-analyte1 signal and the R + P signal for either of the R + P biosensors. However, when looking at ATTO 633 alone, a statistically significant decrease in the signal by ∼2.4% ($p < 0.05$, $N = 3$) was observed between R1 + P1 and R1 + P1 + 10× off-analyte1. However, this statistically-significant difference was not seen in either the fluorescein signal nor the D/A ratio.

Both reporters alone (without probe) were tested against 10× analyte/off-analytes to determine any nonspecific binding effects of the reporters (Supporting Information, Figure S12). For both fluorescein and ATTO 633, neither 10× analyte, 10× off-analyte1, nor 10× off-analyte2 had any effect on the signal of either R1 or R2 ($p > 0.05$, $N = 3$). When considering the D/A ratio, there was no statistical difference between either of the reporters and the 10× analytes/off-analytes apart from R2 + 10× off-analyte1. For R2 + 10× off-analyte1, the D/A ratio increased by ∼5.2% compared to R2 (statistically different with $p < 0.05$, $N = 3$). When looking at the thermodynamic calculations for R2 + off-analyte1, it had a Gibbs energy of −9.1 kcal/mol and a melting temperature of 21.8 °C. Both of these values were much higher than those for R1 + off-analyte1, with a Gibbs energy of −5.9 kcal/mol and a melting temperature of 4.8 °C. Even so, the change in the signal was around 5% with a 10× concentration of off-analyte1, and the changes in signal could not be seen in either the fluorescein or ATTO 633 intensities alone.

Biosensor Sensitivity and Analytical Metrics. Calibration curves were run with both biosensors held at 5 nM in MCF-7 cell lysate. The cell lysate was unfiltered and was used for the experiment at a concentration of 1×10^6 cells per mL. The concentration of the analyte was stepped in 1 nM increments from 0 to 6 nM, and then, an additional solution of 15 nM was added to assess the endpoint of the signal change (Figure 4). A line was fit between 0 and 5 nM analyte to create calibration curves.

Table S6 contains the sensitivity (as analytical slope) and limits of detection (LODs) that were determined from analyzing the calibration curves. The LODs were all found to be in the pM range, with the ATTO 633 signal giving better LODs than the fluorescein signal. The fluorescein signal for R1 + P1 gave an LOD of 209 pM, but the ATTO 633 signal gave 142 pM LOD. The R2 + P2 LODs were lower than those for R1 + P1, with 123 pM for the fluorescein signal and 56 pM for the ATTO 633 signal. These LODs are biologically significant because they are in the middle of the range for raw cell or intracellular miR concentration (fM to nM). From the slopes of the calibration curves, R2 + P2 demonstrated greater sensitivity for the analyte than R1 + P1.

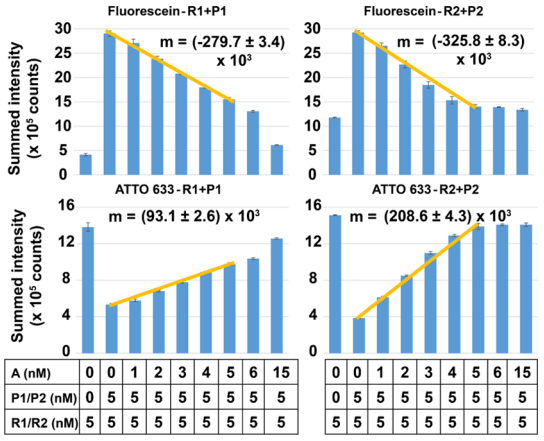

Figure 4. Calibration curves in cell lysate.

CONCLUSIONS

Two reporter + probe biosensors were designed with different toehold locations for hsa-miR-146a-5p. We reported on the susceptibility of each toehold's location to off-analyte binding. Changing the toehold's location on the sensor minimized off-analyte binding because we observed lower amounts of off-analyte binding with R2 + P2 compared to R1 + P1, as determined by signal changes.

The new design strategy started with looking for off-analytes in miRbase to determine the sensor's toehold location that limits off-analyte response. This added consideration will increase the selectivity for future biosensor designs. Off-analyte consideration is important because off-analyte binding leads to false signal generation. False signals lead to false conclusions about a given miR concentration in a sample.

The next step in the design process is to deal with polymorphic regions in the center of the analyte strand. One way to deal with selectivity due to polymorphic regions throughout the analyte strand is to strategically place locked nucleic acids (LNAs) on the probe. The rationale is that LNAs will further separate the thermodynamic stability of probe + analyte and probe + off-analytes and improve sensor selectivity.

The current methods for calculating the thermodynamic parameters for each sensor do not consider the displacement reaction kinetics. Current coarse-grained nucleic-acid prediction models are useful for alleviating this limitation of thermodynamic-only models.[41−54] Future sensors will need to employ both thermodynamic and kinetic models to achieve maximum sensitivity and selectivity at low concentrations. This will be crucial for minimizing the amount of time needed for the sensors to detect their given analyte.

In order to make the sensor design presented here a general method, more sensor designs for different miRs must be tested. From the design perspective, different toehold locations along with different toehold lengths must be tested. Since there are over 1 000 reported miRs with unique sequences, validating the sensor design as a general method will require sensor designers, biostatisticians, and bioinformaticians to come together for establishing a representative sample of miR sequences.

The LODs of both sensors were in the mid-pM range, with the second sensor being slightly better by a factor of ∼1.7 to 2.5. A dynamic range of pM to nM is especially useful because intracellular miR concentrations range from femtomolar to nanomolar. These pM LODs were determined for sensors in MCF-7 cell lysate and showed that the sensor can achieve low detection limits inside a complex sample matrix. Future designs will focus on further decreasing the LODs to get pM or sub-pM. For example, FRET enhancement could be increased by adding more donor dye molecules to the sensor in order to increase the amount of incident energy that can be transferred to the acceptor dye.[55] Additionally, fluorescent species with higher quantum efficiencies, such as quantum dots,[56] can replace the current dye system. As the field progresses, newer

https://dx.doi.org/10.1021/acssensors.9b01968
ACS Sens. 2020, 5, 377−384

molecules such as polymer dots (pdots) or carbon nanodots (c-dots) may be a viable alternative.[57,58]

Future work will focus on transfecting these sensors into cells for intracellular imaging, along with conjugating the biosensor to avidin to aid with tuning intracellular localization. Previous researchers have shown success with electroporation techniques, cell-penetrating peptides, or streptolysin O.[59] To determine transfection efficiency, the biosensors will need internal standard dyes that will not contribute any cross-talk with the reporting dyes or be sensitive to changes in the miR content.[60,61] To combat potential nuclease/protease degradation of our sensors, peptide nucleic acids or morpholinos that have alternative sensor "backbones" may be incorporated into the sensor design.[62−64]

Selectivity of these sensors can be pushed further by adding DNA modifications such as LNAs, described earlier, into the sensors to increase the thermodynamic specificity for a given analyte.[65,66] Noncanonical bases[67] and/or PEG spacers can be incorporated in order to create regions of the sensor with increased specificity. Noncanonical bases will only bind to their corresponding noncanonical pair, making them advantageous in the stem region of the reporter. PEG spacers could increase the length of reporter or probe strands without adding bases that could be susceptible sites for off-target binding. In a recent publication, we showed that PEGs can mask the sensor from endonucleases and off-analyte binding to the reporter.[22]

The multiplexing ability for these sensors could be achieved with different dye-pairs on multiple different reporter + probe complexes detecting different miRs. To decrease cross-talk between multiplexing dyes in solution, molecules with smaller emission profiles such as quantum dots will be required to maximize the amount of dye-pairs that can be used simultaneously.[56] If quantum dots cannot be used, some success has been seen for multiple different dye-labeled probes and mathematical deconvolution to deal with the cross-talk.[68] Other methods to decrease cross-talk between dyes include dye-specific offsets with continuously variable filters in order to detect more dyes in solution.[69]

DNA-nanoassemblies that respond to more than one analyte at a time allow for complex multiplexing.[70] These nanoassemblies are designed to work as logic gates, so that the signal change is only achieved when a particular combination of miRs is present. Overall, considering the toehold location in a sensor will provide researchers a method to improve selectivity for miRs of interest, and maintain sensitivity.

■ ASSOCIATED CONTENT

Supporting Information

The Supporting Information is available free of charge at https://pubs.acs.org/doi/10.1021/acssensors.9b01968.

Parameters and boundary values calculating and predicting chemical equilibria, thermodynamic, and structural metrics; results from miRBase for discovery and analysis of off-analytes; and tables on biosensors' analytical figures of merit (PDF)

■ AUTHOR INFORMATION

Corresponding Author

Sean M. Burrows − *Department of Chemistry, Oregon State University, Corvallis, Oregon 97331, United States;* orcid.org/0000-0001-8296-0459; Email: burrows230@gmail.com

Authors

Nicholas E. Larkey − *Department of Chemistry, Oregon State University, Corvallis, Oregon 97331, United States*

Jessica L. Phillips − *Department of Environmental and Molecular Toxicology, Cancer Research Laboratory, Oregon State University, Corvallis, Oregon 97331, United States*

Hyo Sang Jang − *Department of Environmental and Molecular Toxicology, Cancer Research Laboratory, Oregon State University, Corvallis, Oregon 97331, United States*

Siva K. Kolluri − *Department of Environmental and Molecular Toxicology, Cancer Research Laboratory, Oregon State University, Corvallis, Oregon 97331, United States*

Complete contact information is available at: https://pubs.acs.org/10.1021/acssensors.9b01968

Notes

The authors declare no competing financial interest.

■ ACKNOWLEDGMENTS

The authors would like to thank Oregon State University and the N. L. Tartar Research Fellowship for supporting this research.

■ REFERENCES

(1) Garajová, I.; Ferracin, M.; Porcellini, E.; Palloni, A.; Abbati, F.; Biasco, G.; Brandi, G. Non-Coding RNAs as Predictive Biomarkers to Current Treatment in Metastatic Colorectal Cancer. *Int. J. Mol. Sci.* **2017**, *18*, 1547.

(2) Volinia, S.; Calin, G. A.; Liu, C.-G.; Ambs, S.; Cimmino, A.; Petrocca, F.; Visone, R.; Iorio, M.; Roldo, C.; Ferracin, M.; et al. A MicroRNA Expression Signature of Human Solid Tumors Defines Cancer Gene Targets. *Proc. Natl. Acad. Sci. U.S.A.* **2006**, *103*, 2257−2261.

(3) Zhu, S.; Wu, H.; Wu, F.; Nie, D.; Sheng, S.; Mo, Y.-Y. MicroRNA-21 Targets Tumor Suppressor Genes in Invasion and Metastasis. *Cell Res.* **2008**, *18*, 350−359.

(4) Mitomo, S.; Maesawa, C.; Ogasawara, S.; Iwaya, T.; Shibazaki, M.; Yashima-Abo, A.; Kotani, K.; Oikawa, H.; Sakurai, E.; Izutsu, N.; et al. Downregulation of MiR-138 Is Associated with Overexpression of Human Telomerase Reverse Transcriptase Protein in Human Anaplastic Thyroid Carcinoma Cell Lines. *Cancer Sci.* **2008**, *99*, 280−286.

(5) Visone, R.; Russo, L.; Pallante, P.; De Martino, I.; Ferraro, A.; Leone, V.; Borbone, E.; Petrocca, F.; Alder, H.; Croce, C. M.; et al. MicroRNAs (MiR)-221 and MiR-222, Both Overexpressed in Human Thyroid Papillary Carcinomas, Regulate P27Kip1 Protein Levels and Cell Cycle. *Endocr. Relat. Cancer* **2007**, *14*, 791−798.

(6) Akao, Y.; Nakagawa, Y.; Naoe, T. MicroRNAs 143 and 145 Are Possible Common Onco-MicroRNAs in Human Cancers. *Oncol. Rep.* **2006**, *16*, 845−850.

(7) Shi, B.; Sepp-Lorenzino, L.; Prisco, M.; Linsley, P.; deAngelis, T.; Baserga, R. Micro RNA 145 Targets the Insulin Receptor Substrate-1 and Inhibits the Growth of Colon Cancer Cells. *J. Biol. Chem.* **2007**, *282*, 32582−32590.

(8) Sylvestre, Y.; De Guire, V.; Querido, E.; Mukhopadhyay, U. K.; Bourdeau, V.; Major, F.; Ferbeyre, G.; Chartrand, P. An E2F/MiR-20a Autoregulatory Feedback Loop. *J. Biol. Chem.* **2007**, *282*, 2135−2143.

(9) Shi, X.-B.; Xue, L.; Yang, J.; Ma, A.-H.; Zhao, J.; Xu, M.; Tepper, C. G.; Evans, C. P.; Kung, H.-J.; deVere White, R. W. An Androgen-Regulated MiRNA Suppresses Bak1 Expression and Induces Androgen-Independent Growth of Prostate Cancer Cells. *Proc. Natl. Acad. Sci.* **2007**, *104*, 19983−19988.

(10) Johnson, S. M.; Grosshans, H.; Shingara, J.; Byrom, M.; Jarvis, R.; Cheng, A.; Labourier, E.; Reinert, K. L.; Brown, D.; Slack, F. J.

RAS Is Regulated by the Let-7 MicroRNA Family. *Cell* **2005**, *120*, 635−647.
(11) Fabbri, M.; Garzon, R.; Cimmino, A.; Liu, Z.; Zanesi, N.; Callegari, E.; Liu, S.; Alder, H.; Costinean, S.; Fernandez-Cymering, C.; et al. MicroRNA-29 Family Reverts Aberrant Methylation in Lung Cancer by Targeting DNA Methyltransferases 3A and 3B. *Proc. Natl. Acad. Sci.* **2007**, *104*, 15805−15810.
(12) Shell, S.; Park, S.-M.; Radjabi, A. R.; Schickel, R.; Kistner, E. O.; Jewell, D. A.; Feig, C.; Lengyel, E.; Peter, M. E. Let-7 Expression Defines Two Differentiation Stages of Cancer. *Proc. Natl. Acad. Sci.* **2007**, *104*, 11400−11405.
(13) Giannakakis, A.; Sandaltzopoulos, R.; Greshock, J.; Liang, S.; Huang, J.; Hasegawa, K.; Li, C.; O'Brien-Jenkins, A.; Katsaros, D.; Weber, B. L.; et al. MiR-210 Links Hypoxia with Cell Cycle Regulation and Is Deleted in Human Epithelial Ovarian Cancer. *Cancer Biol. Ther.* **2008**, *7*, 255−264.
(14) Du, Y.; Dong, S. Nucleic Acid Biosensors: Recent Advances and Perspectives. *Anal. Chem.* **2017**, *89*, 189−215.
(15) Graybill, R. M.; Bailey, R. C. Emerging Biosensing Approaches for MicroRNA Analysis. *Anal. Chem.* **2016**, *88*, 431−450.
(16) Yeh, H.-C.; Sharma, J.; Shih, I.-M.; Vu, D. M.; Martinez, J. S.; Werner, J. H. A Fluorescence Light-Up Ag Nanocluster Probe That Discriminates Single-Nucleotide Variants by Emission Color. *J. Am. Chem. Soc.* **2012**, *134*, 11550−11558.
(17) Yeh, H.-C.; Puleo, C. M.; Ho, Y.-P.; Bailey, V. J.; Lim, T. C.; Liu, K.; Wang, T.-H. Tunable Blinking Kinetics of Cy5 for Precise DNA Quantification and Single-Nucleotide Difference Detection. *Biophys. J.* **2008**, *95*, 729−737.
(18) Yeh, H.-C.; Ho, Y.-P.; Wang, T.-H. Quantum dot-mediated biosensing assays for specific nucleic acid detection. *Nanomedicine Nanotechnol. Biol. Med.* **2005**, *1*, 115−121.
(19) Zhang, D. Y.; Seelig, G. Dynamic DNA Nanotechnology Using Strand-Displacement Reactions. *Nat. Chem.* **2011**, *3*, 103−113.
(20) Zhang, D. Y.; Chen, S. X.; Yin, P. Optimizing the Specificity of Nucleic Acid Hybridization. *Nat. Chem.* **2012**, *4*, 208−214.
(21) Larkey, N. E.; Almlie, C. K.; Tran, V.; Egan, M.; Burrows, S. M. Detection of MiRNA Using a Double-Strand Displacement Biosensor with a Self-Complementary Fluorescent Reporter. *Anal. Chem.* **2014**, *86*, 1853−1863.
(22) Lansing, S. S.; Matlapudi, S.; Burrows, S. M. Molecular Approaches To Address the Challenges of RNA Analysis in Complex Matrices. *Anal. Chem.* **2018**, *90*, 9156−9164.
(23) Almlie, C. K.; Larkey, N. E.; Burrows, S. M. Fluorescent MicroRNA Biosensors: A Comparison of Signal Generation to Quenching. *Anal. Methods* **2015**, *7*, 7296−7310.
(24) Larkey, N. E.; Brucks, C. N.; Lansing, S. S.; Le, S. D.; Smith, N. M.; Tran, V.; Zhang, L.; Burrows, S. M. Molecular Structure and Thermodynamic Predictions to Create Highly Sensitive MicroRNA Biosensors. *Anal. Chim. Acta* **2016**, *909*, 109−120.
(25) Larkey, N. E.; Zhang, L.; Lansing, S. S.; Tran, V.; Seewaldt, V. L.; Burrows, S. M. Förster resonance energy transfer to impart signal-on and -off capabilities in a single microRNA biosensor. *Analyst* **2016**, *141*, 6239−6250.
(26) Ning, D.; He, C.; Liu, Z.; Liu, C.; Wu, Q.; Zhao, T.; Liu, R. A Dual-Colored Ratiometric-Fluorescent Oligonucleotide Probe for the Detection of Human Telomerase RNA in Cell Extracts. *Analyst* **2017**, *142*, 1697−1702.
(27) Šulc, P.; Ouldridge, T. E.; Romano, F.; Doye, J. P. K.; Louis, A. A. Modelling Toehold-Mediated RNA Strand Displacement. *Biophys. J.* **2015**, *108*, 1238−1247.
(28) Zavala, V.; Pérez-Moreno, E.; Tapia, T.; Camus, M.; Carvallo, P. MiR-146a and MiR-638 in BRCA1-Deficient Triple Negative Breast Cancer Tumors, as Potential Biomarkers for Improved Overall Survival. *Cancer Biomark.* **2016**, *16*, 99−107.
(29) Sandhu, R.; Rein, J.; D'Arcy, M.; Herschkowitz, J. I.; Hoadley, K. A.; Troester, M. A. Overexpression of MiR-146a in Basal-like Breast Cancer Cells Confers Enhanced Tumorigenic Potential in Association with Altered P53 Status. *Carcinogenesis* **2014**, *35*, 2567−2575.
(30) M'hamed, I. F.; Privat, M.; Ponelle, F.; Penault-Llorca, F.; Kenani, A.; Bignon, Y.-J. Identification of MiR-10b, MiR-26a, MiR-146a and MiR-153 as Potential Triple-Negative Breast Cancer Biomarkers. *Cell. Oncol.* **2015**, *38*, 433−442.
(31) Li, Y.; Xu, Y.; Yu, C.; Zuo, W. Associations of MiR-146a and MiR-146b Expression and Breast Cancer in Very Young Women. *Cancer Biomark* **2015**, *15*, 881−887.
(32) Saferding, V.; Puchner, A.; Goncalves-Alves, E.; Hofmann, M.; Bonelli, M.; Brunner, J. S.; Sahin, E.; Niederreiter, B.; Hayer, S.; Kiener, H. P.; et al. MicroRNA-146a Governs Fibroblast Activation and Joint Pathology in Arthritis. *J. Autoimmun.* **2017**, *82*, 74−84.
(33) Zuker, M. Mfold Web Server for Nucleic Acid Folding and Hybridization Prediction. *Nucleic Acids Res.* **2003**, *31*, 3406−3415.
(34) Bioinformatics. *Methods in Molecular Biology*; Keith, J. M., Ed.; Humana: Totowa, NJ, 2008.
(35) Griffiths-Jones, S. miRBase: microRNA sequences, targets and gene nomenclature. *Nucleic Acids Res.* **2006**, *34*, D140−D144.
(36) Griffiths-Jones, S.; Saini, H. K.; van Dongen, S.; Enright, A. J. miRBase: tools for microRNA genomics. *Nucleic Acids Res.* **2007**, *36*, D154−D158.
(37) Kozomara, A.; Griffiths-Jones, S. MiRBase: Integrating MicroRNA Annotation and Deep-Sequencing Data. *Nucleic Acids Res.* **2011**, *39*, D152−D157.
(38) Lee, H.; Shapiro, S. J.; Chapin, S. C.; Doyle, P. S. Encoded Hydrogel Microparticles for Sensitive and Multiplex MicroRNA Detection Directly from Raw Cell Lysates. *Anal. Chem.* **2016**, *88*, 3075−3081.
(39) Zhang, Z.; Fan, T. W.; Hsing, I.-M. Integrating DNA Strand Displacement Circuitry to the Nonlinear Hybridization Chain Reaction. *Nanoscale* **2017**, *9*, 2748−2754.
(40) SantaLucia, J. A Unified View of Polymer, Dumbbell, and Oligonucleotide DNA Nearest-Neighbor Thermodynamics. *Proc. Natl. Acad. Sci.* **1998**, *95*, 1460−1465.
(41) Wiese, K. C.; Hendriks, A. Comparison of P-RnaPredict and Mfold–Algorithms for RNA Secondary Structure Prediction. *Bioinformatics* **2006**, *22*, 934−942.
(42) Zhang, D. Y.; Winfree, E. Control of DNA Strand Displacement Kinetics Using Toehold Exchange. *J. Am. Chem. Soc.* **2009**, *131*, 17303−17314.
(43) Ouldridge, T. E.; Louis, A. A.; Doye, J. P. K. Structural, Mechanical, and Thermodynamic Properties of a Coarse-Grained DNA Model. *J. Chem. Phys.* **2011**, *134*, 085101.
(44) Šulc, P.; Romano, F.; Ouldridge, T. E.; Rovigatti, L.; Doye, J. P.; Louis, A. A. Sequence-Dependent Thermodynamics of a Coarse-Grained DNA Model. *J. Chem. Phys.* **2012**, *137*, 135101.
(45) Doye, J. P. K.; Ouldridge, T. E.; Louis, A. A.; Romano, F.; Šulc, P.; Matek, C.; Snodin, B. E. K.; Rovigatti, L.; Schreck, J. S.; Harrison, R. M.; et al. Coarse-Graining DNA for Simulations of DNA Nanotechnology. *Phys. Chem. Chem. Phys.* **2013**, *15*, 20395−20414.
(46) Ouldridge, T. E.; Šulc, P.; Romano, F.; Doye, J. P. K.; Louis, A. A. DNA Hybridization Kinetics: Zippering, Internal Displacement and Sequence Dependence. *Nucleic Acids Res.* **2013**, *41*, 8886−8895.
(47) Ouldridge, T. E.; Hoare, R. L.; Louis, A. A.; Doye, J. P. K.; Bath, J.; Turberfield, A. J. Optimizing DNA Nanotechnology through Coarse-Grained Modeling: A Two-Footed DNA Walker. *ACS Nano* **2013**, *7*, 2479−2490.
(48) Šulc, P.; Romano, F.; Ouldridge, T. E.; Doye, J. P.; Louis, A. A. A Nucleotide-Level Coarse-Grained Model of RNA. *J. Chem. Phys.* **2014**, *140*, 235102.
(49) Srinivas, N.; Ouldridge, T. E.; Šulc, P.; Schaeffer, J. M.; Yurke, B.; Louis, A. A.; Doye, J. P. K.; Winfree, E. On the Biophysics and Kinetics of Toehold-Mediated DNA Strand Displacement. *Nucleic Acids Res.* **2013**, *41*, 10641−10658.
(50) Potoyan, D. A.; Savelyev, A.; Papoian, G. A. Recent successes in coarse-grained modeling of DNA. *Wiley Interdiscip. Rev. Comput. Mol. Sci.* **2013**, *3*, 69−83.
(51) Machinek, R. R. F.; Ouldridge, T. E.; Haley, N. E. C.; Bath, J.; Turberfield, A. J. Programmable Energy Landscapes for Kinetic Control of DNA Strand Displacement. *Nat. Commun.* **2014**, *5*, 5324.

https://dx.doi.org/10.1021/acssensors.9b01968
ACS Sens. 2020, 5, 377−384

(52) Boniecki, M. J.; Lach, G.; Dawson, W. K.; Tomala, K.; Lukasz, P.; Soltysinski, T.; Rother, K. M.; Bujnicki, J. M. SimRNA: A Coarse-Grained Method for RNA Folding Simulations and 3D Structure Prediction. *Nucleic Acids Res.* **2016**, *44*, No. e63.
(53) Bell, D. R.; Cheng, S. Y.; Salazar, H.; Ren, P. Capturing RNA Folding Free Energy with Coarse-Grained Molecular Dynamics Simulations. *Sci. Rep.* **2017**, *7*, 45812.
(54) Benson, E.; Lolaico, M.; Tarasov, Y.; Gådin, A.; Högberg, B. Evolutionary Refinement of DNA Nanostructures Using Coarse-Grained Molecular Dynamics Simulations. *ACS Nano* **2019**, *13*, 12591−12598.
(55) Buckhout-White, S.; Spillmann, C. M.; Algar, W. R.; Khachatrian, A.; Melinger, J. S.; Goldman, E. R.; Ancona, M. G.; Medintz, I. L. Assembling Programmable FRET-Based Photonic Networks Using Designer DNA Scaffolds. *Nat. Commun.* **2014**, *5*, 1−16.
(56) Gliddon, H. D.; Howes, P. D.; Kaforou, M.; Levin, M.; Stevens, M. M. A Nucleic Acid Strand Displacement System for the Multiplexed Detection of Tuberculosis-Specific MRNA Using Quantum Dots. *Nanoscale* **2016**, *8*, 10087−10095.
(57) Wu, C.; Chiu, D. T. Highly Fluorescent Semiconducting Polymer Dots for Biology and Medicine. *Angew. Chem., Int. Ed.* **2013**, *52*, 3086−3109.
(58) Noh, E.-H.; Ko, H. Y.; Lee, C. H.; Jeong, M.-S.; Chang, Y. W.; Kim, S. Carbon Nanodot-Based Self-Delivering MicroRNA Sensor to Visualize MicroRNA124a Expression during Neurogenesis. *J. Mater. Chem. B* **2013**, *1*, 4438−4445.
(59) Chen, A. K.; Behlke, M. A.; Tsourkas, A. Efficient Cytosolic Delivery of Molecular Beacon Conjugates and Flow Cytometric Analysis of Target RNA. *Nucleic Acids Res.* **2008**, *36*, No. e69.
(60) Chen, A. K.; Davydenko, O.; Behlke, M. A.; Tsourkas, A. Ratiometric Bimolecular Beacons for the Sensitive Detection of RNA in Single Living Cells. *Nucleic Acids Res.* **2010**, *38*, No. e148.
(61) Zhang, X.; Song, Y.; Shah, A. Y.; Lekova, V.; Raj, A.; Huang, L.; Behlke, M. A.; Tsourkas, A. Quantitative Assessment of Ratiometric Bimolecular Beacons as a Tool for Imaging Single Engineered RNA Transcripts and Measuring Gene Expression in Living Cells. *Nucleic Acids Res.* **2013**, *41*, No. e152.
(62) Borgatti, M.; Romanelli, A.; Saviano, M.; Pedone, C.; Lampronti, I.; Breda, L.; Nastruzzi, C.; Bianchi, N.; Mischiati, C.; Gambari, R. Resistance of Decoy PNA-DNA Chimeras to Enzymatic Degradation in Cellular Extracts and Serum. *Oncol. Res.* **2003**, *13*, 279−287.
(63) Wang, G.; Xu, X. S. Peptide Nucleic Acid (PNA) Binding-Mediated Gene Regulation. *Cell Res.* **2004**, *14*, 111−116.
(64) Hudziak, R. M.; Barofsky, E.; Barofsky, D. F.; Weller, D. L.; Huang, S.-B.; Weller, D. D. Resistance of Morpholino Phosphorodiamidate Oligomers to Enzymatic Degradation. *Antisense Nucleic Acid Drug Dev* **1996**, *6*, 267−272.
(65) Wang, L.; Yang, C. J.; Medley, C. D.; Benner, S. A.; Tan, W. Locked Nucleic Acid Molecular Beacons. *J. Am. Chem. Soc.* **2005**, *127*, 15664−15665.
(66) Martinez, K.; Estevez, M.-C.; Wu, Y.; Phillips, J. A.; Medley, C. D.; Tan, W. Locked Nucleic Acid Based Beacons for Surface Interaction Studies and Biosensor Development. *Anal. Chem.* **2009**, *81*, 3448−3454.
(67) Johnson, S. C.; Sherrill, C. B.; Marshall, D. J.; Moser, M. J.; Prudent, J. R. A Third Base Pair for the Polymerase Chain Reaction: Inserting IsoC and IsoG. *Nucleic Acids Res.* **2004**, *32*, 1937−1941.
(68) Liu, Y.; Wei, M.; Li, Y.; Liu, A.; Wei, W.; Zhang, Y.; Liu, S. Application of Spectral Crosstalk Correction for Improving Multiplexed MicroRNA Detection Using a Single Excitation Wavelength. *Anal. Chem.* **2017**, *89*, 3430−3436.
(69) Almlie, C. K.; Hsiao, A.; Burrows, S. M. Dye-Specific Wavelength Offsets to Resolve Spectrally Overlapping and Co-Localized Two-Photon Induced Fluorescence. *Anal. Chem.* **2016**, *88*, 1462−1467.
(70) Zhang, L.; Bluhm, A. M.; Chen, K.-J.; Larkey, N. E.; Burrows, S. M. Performance of Nano-Assembly Logic Gates with a DNA Multi-Hairpin Motif. *Nanoscale* **2017**, *9*, 1709−1720.

https://dx.doi.org/10.1021/acssensors.9b01968
ACS Sens. 2020, 5, 377−384